Experimental Thermal and Fluid Science 68 (2015) 711–721

Contents lists available at ScienceDirect

Experimental Thermal and Fluid Science

journal homepage: www.elsevier.com/locate/etfs

Two-dimensional bubble clustering in hydraulic jumps

Hang Wang *, Zhifang Hu, Hubert Chanson

The University of Queensland, School of Civil Engineering, Brisbane, QLD 4072, Australia

ARTICLE INFO

Article history:
Received 19 January 2015
Received in revised form 8 July 2015
Accepted 8 July 2015
Available online 17 July 2015

Keywords:
Bubble clusters
Two-phase flow
Bubble–turbulence interaction
Two-dimensional clustering
Near-wake criterion
Air entrainment

ABSTRACT

Hydraulic jumps are characterised by turbulent flow structures and air entrainment. As a result of the turbulence–bubble interaction, non-random bubble distributions are observed in the bubble transport processes, forming bubble clusters. This paper presents a physical investigation of bubble/droplet clustering events in hydraulic jumps based upon a two-dimensional near-wake clustering criterion. Clusters were identified with consideration of bubble–bubble interplay in both longitudinal and transverse directions. In the highly-aerated flow region of the roller, more than 50% of bubbles were advected in two-dimensional clusters. Though the largest percentage of clusters was formed by two bubbles, over 10% of clusters were large two-dimensional cluster structures consisting of six bubbles or more. Clustering properties such as cluster production rate, average cluster size and clustered particle size distributions were analysed and their spatial distributions were presented for an inflow Froude number 7.5 with various Reynolds numbers from 3.4×10^4 to 1.4×10^5. All clustering properties decreased in the longitudinal direction as the turbulence dissipated and flow de-aerated. Comparison between the one-dimensional and two-dimensional clustering criteria was discussed along with their limitations. The quantification of the clustering properties provided a valuable measure of the correlation between air entrainment and turbulence development in such complex air–water flows.

1. Introduction

A hydraulic jump is a complex two-phase open channel flow with air entrainment into water. A jump roller forms at the transition between the supercritical approach flow and the subcritical downstream water body, yielding to a sudden increase in flow depth and extremely turbulent flow structures in the roller [14,23]. Air is entrapped both at the impingement point (jump toe) and through the free-surface of the roller (Fig. 1a). Such a combination of singular and interfacial aeration processes is typical for a partially-developed inflow condition with limited inflow self-aeration [24,3]. The transport of entrained bubbles interacts strongly with the growth and dissipation of turbulence in the roller. For example, some macro-scale bubble–turbulence interplay is visible in Fig. 1a, showing a large amount of bubbles entrapped in large vortical structures and advected downstream. Fig. 1b highlights the bubbly and splashing flow structures next to the free-surface, where clusters of bubbles/droplets can be seen. Further micro-scale turbulence modulation and bubble re-grouping were observed by means of two-phase flow measurements. The bubble–turbulence and bubble–bubble interactions introduce non-randomness and anisotropy to the bubble convection and diffusion processes, which can be of particular interest in terms of understanding of flow mechanics, validation of numerical modelling and application of hydraulic jump, e.g. as a fluid mixer in chemical and water treatment plants.

The physical study of bubble clustering events in an intense turbulent flow relies largely upon the bubble detection technique. For decades the most successful measurements of detailed air–water flow characteristics in hydraulic jumps were performed using intrusive phase-detection needle probes [22,7,19]. The successive detection of air–water interfaces at a fixed location allowed for basic bubble/droplet clustering analysis along the flow direction. At the given measurement location, one-dimensional (i.e. longitudinal) clusters were identified based upon a defined clustering criterion, and clustering properties such as the formation rate and average size of clusters were analysed [4,12,2]. Similar studies of clustering events were not only restricted to hydraulic jumps, but also conducted for dropshaft jets and stepped spillway flows [9,11,10]. Despite the limitation inherent to the one-dimensional analysis, the results hinted that the clustering index may provide a measure of the vorticity production rate and associated energy dissipation [1,25].

In a recent contribution of Sun and Chanson [25], a cluster identification criterion was developed into two-dimensions with

* Corresponding author. Tel.: +61 4309 49204.
E-mail address: hang.wang@uqconnect.edu.au (H. Wang).

http://dx.doi.org/10.1016/j.expthermflusci.2015.07.006
0894-1777/

Nomenclature

C	time-averaged void fraction
C_{max}	local maximum void fraction in shear flow region
d_1	inflow water depth (m)
F	bubble/droplet count rate (Hz)
F_{clu}	cluster count rate (Hz)
$(F_{clu})_{max}$	maximum cluster count rate in shear flow region (Hz)
F_{max}	maximum bubble count rate in shear flow region (Hz)
Fr_1	inflow Froude number, $Fr_1 = V_1/\sqrt{g \times d_1}$
g	gravity acceleration (m/s^2)
h	upstream gate opening (m)
N_{clu}	cluster size defined as the number of particles in a cluster
P_{clu}	cluster proportion defined as the percentage of particles involved in clustering
Q	flow rate (m^3/s)
Re	Reynolds number, $Re = \rho \times V_1 \times d_1/\mu$
$(t_{cent})_a$	air chord time centre (s)
$(t_{cent})_w$	water chord time centre (s)
$(t_{ch})_a$	air chord time (s)
$(t_{ch})_w$	water chord time (s)
V_1	cross-sectional average inflow velocity (m/s)
x	longitudinal distance from the upstream gate (m)
x_1	longitudinal position of jump toe (m)
Y_{Fmax}	characteristic elevation of maximum bubble count rate in shear flow region (m)
Y_{90}	characteristic elevation where $C = 0.9$ (m)
y	vertical distance from the channel bed (m)
z	transverse distance from the channel centreline (m)
Δz	transverse separation distance between two phase-detection probe sensors (m)
λ	dimensionless coefficient of near-wake length scale
μ	water dynamic viscosity (Pa s)
ρ	water density (kg/m^3)
ω	dimensionless coefficient for side-by-side particle clustering characterisation

Superscript

(l)	property of leading particle
(t)	property of trailing particle
(1)	property of one-dimensional clusters measured on the channel centreline
(2)	property of two-dimensional clusters

consideration of longitudinal clusters, side-by-side clusters and their combination in a horizontal plane. The two-dimensional clustering analysis was applied to a stepped spillway flow, where the bubbles travelling side by side were detected by two simultaneously sampled phase-detection sensors. Their work brought the research of bubble clustering in air–water free-surface flow to the cutting edge, though no further investigation was undertaken in other types of flows because of the limited existing data. In this paper, the two-dimensional criterion was refined and applied to hydraulic jumps. New experimental data were collected in hydraulic jumps for four Reynolds numbers from 3.4×10^4 to 1.4×10^5 with an identical inflow Froude number $Fr_1 = 7.5$. The two-dimensional near-wake clustering criterion was introduced first, followed by a description of experimental facility and instrumentation. The results are presented in terms of basic air–water flow properties including the void fraction and bubble count rate, and clustering properties including the cluster count rate, cluster size, cluster proportion and clustered bubble chord time. For each clustering property, results derived from two-dimensional criterion are compared with those given by one-dimensional criterion. The scale effects associated with a range of Reynolds numbers and the uncertainties of cluster identification are discussed at the end.

2. Two-dimensional near-wake clustering criterion

The existence of non-random particle grouping (air bubble or water droplet clusters) may be implied by comparison between the probability density function of inter-particle arrival time and Poisson distribution [13,4]. Let us define, in the bubbly flow region, the air chord time $(t_{ch})_a$ as the time that an air bubble spent on the phase-detection probe sensor tip, and the water chord time $(t_{ch})_w$ as the time that the sensor tip was in water between two adjacent bubbles. In the spray region above the bubbly flow, the water chord time refers to the time that a water droplet spends on the sensor tip, and the air chord time to the time of the sensor tip being in air between two droplets. The one-dimensional clusters were defined using criteria that compared the inter-particle chord time with some pre-defined measure. This measure could be a constant value, a statistical particle interval or a dimension of the leading particle itself [9,4]. In the present study, a near-wake criterion was adopted to better reflect the interplay between neighbouring bubbles travelling one after the other [6]. That is, a longitudinal bubble cluster was defined when:

$$(t_{ch})_w < \lambda \times (t_{ch})_a^{(l)} \quad (1)$$

where the superscript (l) denotes the leading particle and the coefficient λ is a dimensionless near-wake length scale. For pseudo-spherical particles, the value of λ may range between 0.5 and 2. Herein $\lambda = 1$ was applied following a number of studies on one-dimensional clusters. Eq. (1) implied that the trailing bubble was in the near-wake of the leading bubble [6,12].

Given a careful determination of the transverse separation Δz between two side-by-side measurement locations, a two-dimensional, side-by-side bubble cluster was defined with reference to the lag time between the bubble chord time centres:

$$\left|(t_{cent})_a^{(l)} - (t_{cent})_a^{(t)}\right| < \omega \times \max\left((t_{ch})_a^{(l)}, (t_{ch})_a^{(t)}\right) \quad (2)$$

where $(t_{cent})_a$ is the air bubble chord time centre, as sketched in Fig. 2, the superscripts (l) and (t) referring to the leading and side-by-side trailing bubbles respectively, and ω is a coefficient characterising the proximity of side-by-side particles. A sensitivity study indicated that the number of identified side-by-side bubble clusters increased with increasing value of ω from 0.3 to 0.8 [25]. A selection of $\omega = 0.5$ implied a chord time centre of the smaller bubble within the chord time span of the larger bubble that travelled beside (Fig. 2), which was applied in Sun and Chanson [25] as well as in the present study.

A combination of Eqs. (1) and (2) does define the two-dimensional bubble clusters in a horizontal plane for a given transverse separation Δz. Fig. 2 illustrates the detection of some two-dimensional bubble clusters with two phase-detection probe sensors. In Fig. 2, $\lambda = 1$ and $\omega = 0.5$ were applied as for all the remaining analysis.

In the free-surface region, a similar series of criteria defines the two-dimensional water droplet clusters:

$$(t_{ch})_a < \lambda \times (t_{ch})_w^{(l)} \quad (3)$$

$$\left|(t_{cent})_w^{(l)} - (t_{cent})_w^{(t)}\right| < \omega \times \max\left((t_{ch})_w^{(l)}, (t_{ch})_w^{(t)}\right) \quad (4)$$

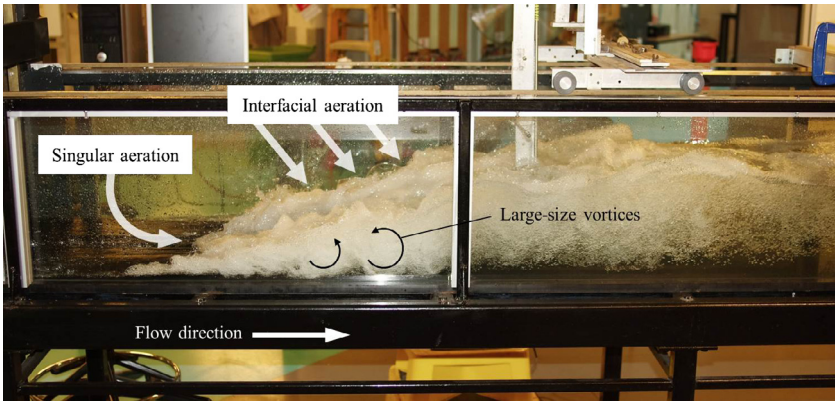

(a) *Side view of the jump roller*

(b) *Details of air-water structures and droplets at the roller surface (high-shutter-speed photograph)*

Fig. 1. Air entrainment and macro-scale bubble–turbulence interaction in strong hydraulic jump with partially-developed inflow conditions (see Test 2 in Table 1 for flow conditions).

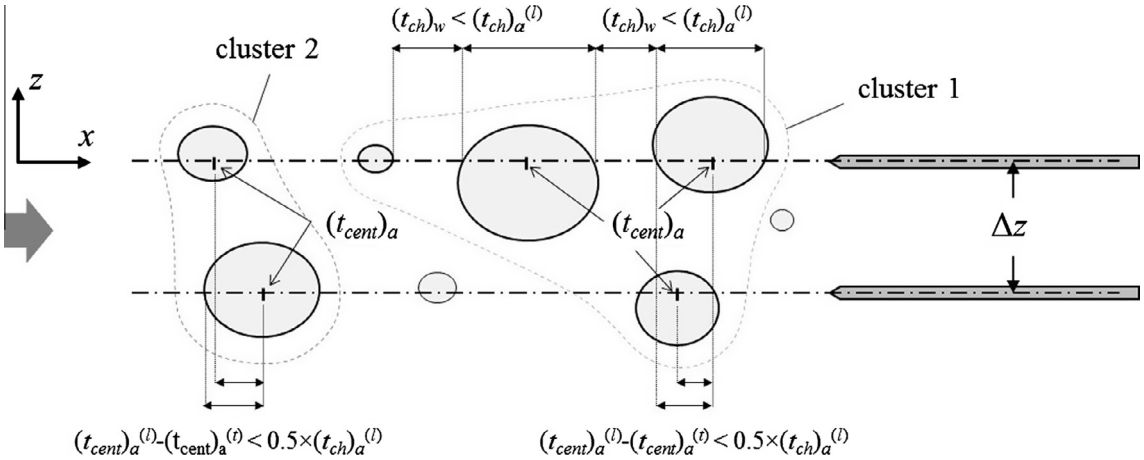

Fig. 2. Top-view sketch of detection of two-dimensional bubble clusters by side-by-side phase-detection needle sensors; flow from left to right.

with $(t_{cent})_w^{(l)}$ and $(t_{cent})_w^{(t)}$ being the water chord time centres of leading and trailing droplets. Note that one particle could only belong to one cluster, and a two-dimensional cluster might consist of one or more longitudinal cluster, side-by-side cluster or combination of both. Fig. 3 presents a limited number of examples of two-dimensional cluster structures. The identification of

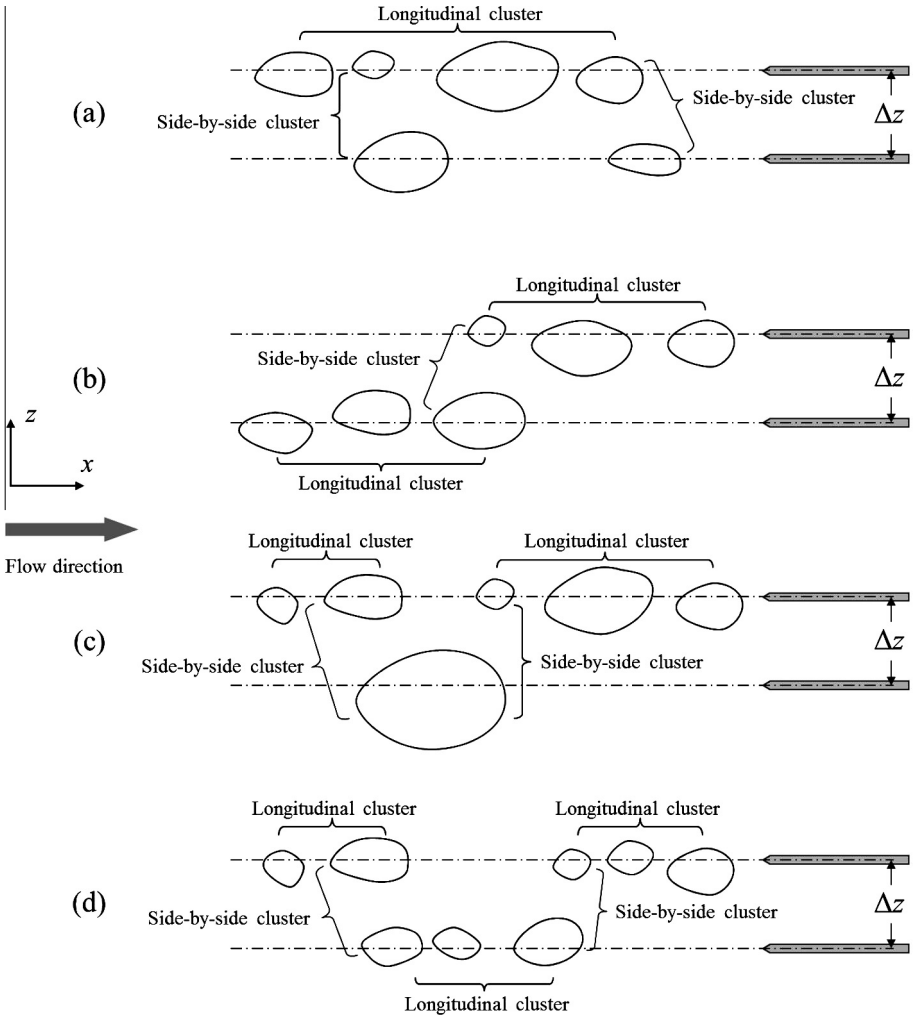

Fig. 3. Example of typical two-dimensional cluster structures.

two-dimensional clusters was much more complicated than that of one-dimensional clusters. The analysis was based upon a primary processing of the signals of each phase-detection probe sensor, focusing on the longitudinal clustering given by each sensor respectively, and a logical merge of the two processed signals. This method involved a logical determination of the start and end of a two-dimensional cluster, thus ensuring all possible combinations of one-dimensional clusters to be covered and no particles were double counted.

3. Experimental facility, instrumentation and flow conditions

New experiments were performed in a horizontal rectangular channel built with 3.2-m long, 0.5-m wide smooth HDPE bed and 0.4-m high glass sidewalls. The hydraulic jumps were generated by a horizontal approach flow that was discharged into the flume from a head tank equipped with a rounded undershoot gate (Fig. 4). The tailwater conditions were controlled by a downstream overshoot gate, set at a relevant elevation to force the jump toe at a mean position $x = x_1$, where x is the longitudinal distance from the upstream gate (Fig. 4). The flow rate was measured using a Venturi meter installed in the supply pipeline and calibrated on site. Fig. 4 shows a simplified sketch of the channel and the experimental flow.

Two conductivity phase-detection probes were used for the air–water flow measurements. The needle sensor of the probe was designed to pierce the bubbles and droplets, and instantaneous void fraction was recorded in voltage signal corresponding to the different electric resistance of air and water. Each sensor consisted of a 0.25-mm diameter needle and was excited by an electronic system allowing for a response time less than 10 μs. The two phase-detection sensors were mounted parallel at identical longitudinal and vertical positions, separated by a controlled transverse distance Δz (Fig. 2). Herein $\Delta z = 3.57$ mm was applied, and the selection of Δz is discussed in Section 7. Measurements were performed at several vertical cross-sections on the channel centreline, the elevation of the probes being monitored with a magnetic digital scale with accuracy within 0.1 mm. At each location, the two sensors were scanned simultaneously at 20 kHz per sensor for 45 s.

Table 1 summarises the flow conditions for the present study. For all investigations, the inflow Froude number was $Fr_1 = 7.5$ and the inflow length fulfilled $h/x_1 = 0.024$, h being the undershoot gate opening. Four Reynolds numbers were investigated. Herein the Froude and Reynolds numbers were defined using the inflow depth d_1 measured immediately upstream of jump toe (Fig. 4), and all tests were characterised by partially-developed inflow conditions [26].

4. Basic air–water flow properties

At large Froude numbers, a hydraulic jump is characterised by a marked roller, a highly turbulent motion with macro-scale

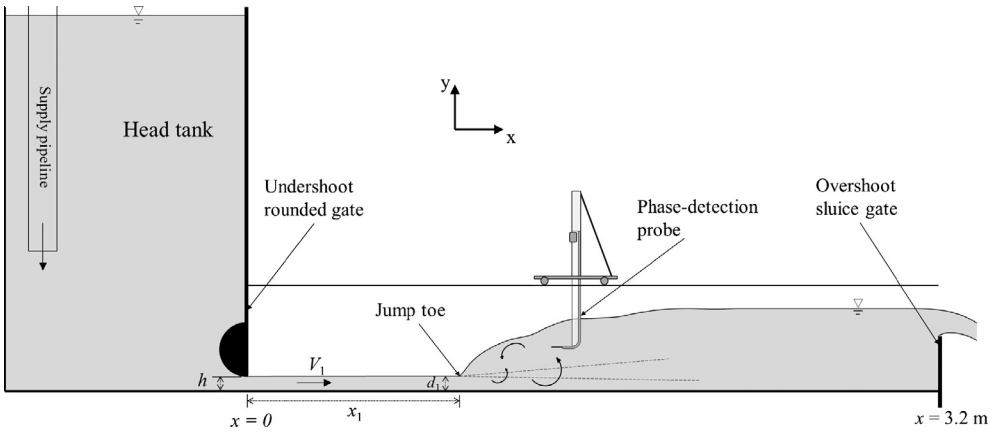

Fig. 4. Sketch of experimental channel and key parameters of flow conditions.

Table 1
Experimental flow conditions (present study).

Test	Q (m^3/s)	h (m)	x_1 (m)	d_1 (m)	Fr_1	Re
1	0.0172	0.012	0.50	0.0129	7.5	3.4×10^4
2	0.0347	0.020	0.83	0.0206	7.5	6.8×10^4
3	0.0530	0.025	1.04	0.0273	7.5	1.1×10^5
4	0.0705	0.030	1.25	0.033	7.5	1.4×10^5

Notes: Q: flow rate; h: upstream gate opening; x_1: longitudinal jump toe position; d_1: inflow depth; Fr_1: inflow Froude number; Re: inflow Reynolds number.

vortices, significant kinetic energy dissipation and air entrainment [15,18]. A characteristic feature of the jump is the large amount of entrained air bubbles seen in Fig. 1a. Herein basic air–water flow properties were measurements with the phase-detection probe signal and these included the time-averaged void fraction C and bubble count rate F. Fig. 5 presents the vertical distributions of C and F at five cross-sections on the roller centreline for Test 2. In Fig. 5, the free-surface profile is plotted at the elevation Y_{90} where $C = 0.9$. The results highlighted a turbulent shear layer in the lower part of roller, with the presence of a local maximum void fraction C_{max} and a maximum bubble count rate F_{max}. The maximum void fraction was observed consistently at a higher location than the maximum bubble count rate, and both maximum values decreased with increasing distance from the jump toe. In the free-surface region above, the void fraction increased monotonically to unity in air, and the bubble count rate exhibited a secondary peak around the position with $C = 0.3$–0.4 [26]. The typical void fraction and bubble count rate distributions were consistent with previous data: e.g. Chanson and Brattberg [7] using intrusive conductivity phase-detection probe and Murzyn et al. [21] using optical fibre probe. While the turbulent shear layer was characterised by the advection of large-size vortices and large amount of entrained bubbles, the free-surface region was observed with flow recirculation and air–water exchange between the bubbly flow and the upper spray region.

5. Clustering properties

The clustering properties were investigated in terms of the cluster count rate F_{clu} defined as the number of clusters per second, the cluster size N_{clu} defined as the number of particles per cluster, and the cluster proportion P_{clu} defined as the ratio of the number of particles in clusters to the total number of particles. Superscripts (1) and (2) are used to denote the parameters derived for one-dimensional and two-dimensional clusters respectively. The longitudinal clustering properties were measured with one of the phase-detection probe sensors on the channel centreline. The parameters were considered to characterise bubble clustering in the bubbly flow with void fraction $0 < C < 0.3$, and to characterise the droplet clustering in the spray region with $0.7 < C < 1$.

5.1. Cluster count rate

Fig. 6a–c present the vertical distributions of dimensionless cluster count rates at three longitudinal positions for Test 2. The data derived from the two-dimensional clustering criterion $F_{clu}^{(2)} \times d_1/V_1$ are compared with the data of longitudinal clusters $F_{clu}^{(1)} \times d_1/V_1$ and the time-averaged void fraction C. The cluster refers to the bubble cluster for $C < 0.3$ and droplet cluster for $C > 0.7$. Both two-dimensional and one-dimensional cluster count rate profiles showed similar shapes to the bubble count rate profile, e.g. as presented in Fig. 5. That is, a maximum cluster count

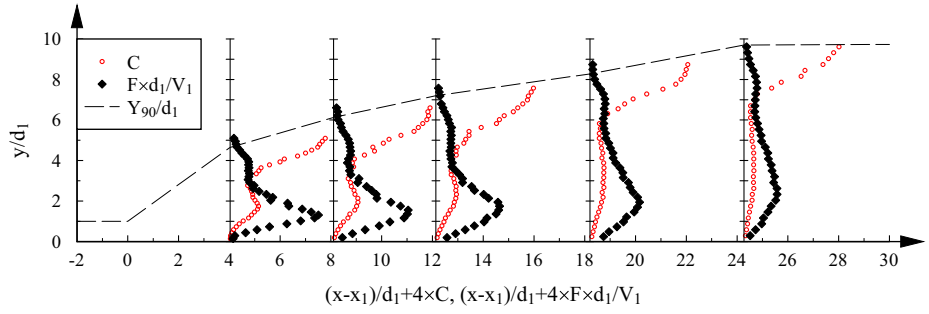

Fig. 5. Time-averaged void fraction and bubble count rate distributions in jump roller for Test 2 ($Fr_1 = 7.5$, $Re = 6.8 \times 10^4$), dash line denoting the free-surface elevation Y_{90} (see Table 1 for detailed flow conditions).

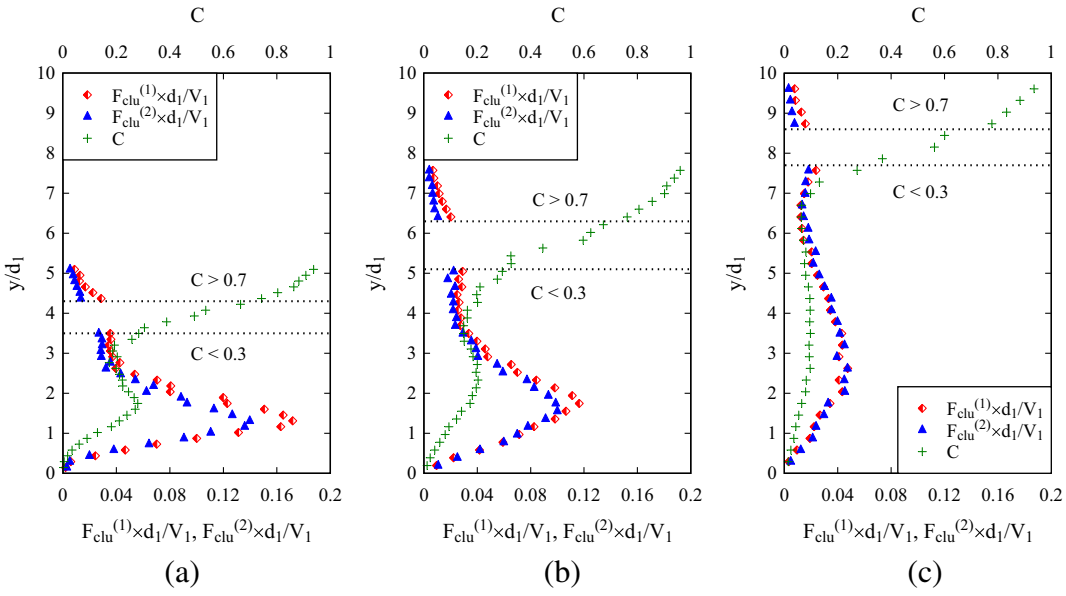

Fig. 6. Vertical distributions of longitudinal and two-dimensional cluster count rates with comparison to time-averaged void fraction for Test 2 ($Fr_1 = 7.5$, $Re = 6.8 \times 10^4$): (a) $(x - x_1)/d_1 = 4.15$; (b) $(x - x_1)/d_1 = 12.5$; (c) $(x - x_1)/d_1 = 25$.

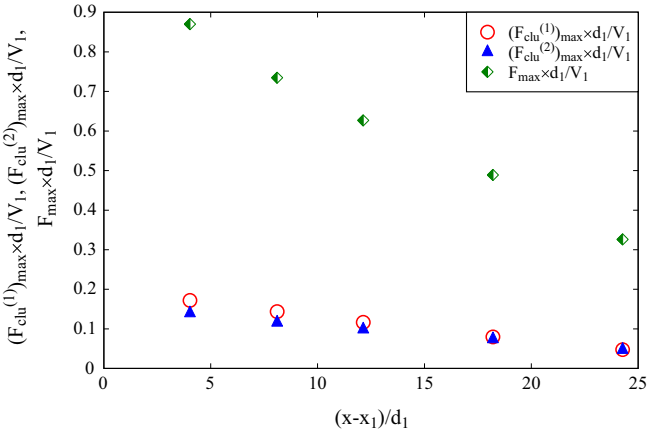

Fig. 7. Longitudinal distributions of maximum cluster count rates in turbulent shear layer for Test 2 ($Fr_1 = 7.5$, $Re = 6.8 \times 10^4$), with comparison to maximum bubble count rate.

rate was exhibited in the turbulent shear layer, with decreasing maximum values along the longitudinal downstream direction. Fig. 7 shows the longitudinal decay of the maximum bubble cluster count rates for Test 2, with comparison to the corresponding maximum bubble count rate. Figs. 6 and 7 indicate that, at a given longitudinal position downstream of the toe, the two-dimensional cluster count rate $F_{clu}^{(2)}$ was consistently smaller than the longitudinal cluster count rate $F_{clu}^{(1)}$ through the vertical cross-section, and both smaller than the bubble count rate: i.e. $F_{clu}^{(2)} < F_{clu}^{(1)} < F$. Comparing the one-dimensional and two-dimensional clusters, the effects of the introduction of transverse clustering were two-fold. On the one hand, the cluster count rate could increase because of the inclusion of side-by-side clusters that were not involved in longitudinal clustering. On the other hand, the cluster count rate could be reduced because the particles in side-by-side clusters might interact with more than one longitudinal cluster hence merge these clusters into one. The present results indicated that the latter factor was predominant hence the cluster count rate was overall reduced by taking into account the side-by-side clusters. The largest difference between $F_{clu}^{(2)}$ and $F_{clu}^{(1)}$ was found close to the jump toe, implying more frequent transverse particle interactions for which the simple one-dimensional consideration might not be sufficient.

Wang [26] performed some comparative analysis between the longitudinal cluster count rate and bubble count rate for a wide range of Froude and Reynolds numbers. The results suggested a power equation followed by the maximum longitudinal cluster count rate and maximum bubble count rate:

$$\frac{(F_{clu}^{(1)})_{max} \times d_1}{V_1} = 0.183 \times \left(\frac{F_{max} \times d_1}{V_1}\right)^{1.33}$$
$$\text{for } 3.8 < Fr_1 < 10 \text{ and } 3.4 \times 10^4 < Re < 1.6 \times 10^5 \quad (5)$$

Eq. (5) implied a more rapid longitudinal decay in cluster count rate than in bubble count rate in the shear flow, corresponding to a more rapid dissipation of turbulent structures than the flow de-aeration process. The present and previous studies also showed the same vertical positions for the presence of maximum cluster count rate and maximum bubble count rate at $y = Y_{Fmax}$ in the shear layer.

5.2. Cluster size and cluster proportion

The cluster size refers to the number of particles in a cluster, and the cluster proportion is the percentage of particles in clusters. According to the definitions, the average cluster size N_{clu} and the cluster proportion P_{clu} satisfy:

$$P_{clu} = \frac{F_{clu}}{F} \times N_{clu} \quad (6)$$

where F is the bubble/droplet count rate, F_{clu} is the cluster count rate and $N_{clu} \geqslant 2$. For the cluster count rate quasi-proportional to the bubble/droplet count rate, the profiles of average cluster size and cluster proportion were expected in similar shapes. Fig. 8 presents the vertical distributions of average cluster size and cluster proportion for longitudinal and two-dimensional clusters in the same flow (Test 2). The data were compared with the time-averaged void fraction, showing comparable profile shapes in the bubbly flow ($C < 0.3$). Both cluster sizes and proportions exhibited local maximum values in the shear layer around the characteristic elevation of maximum void fraction Y_{Cmax}. The maximum

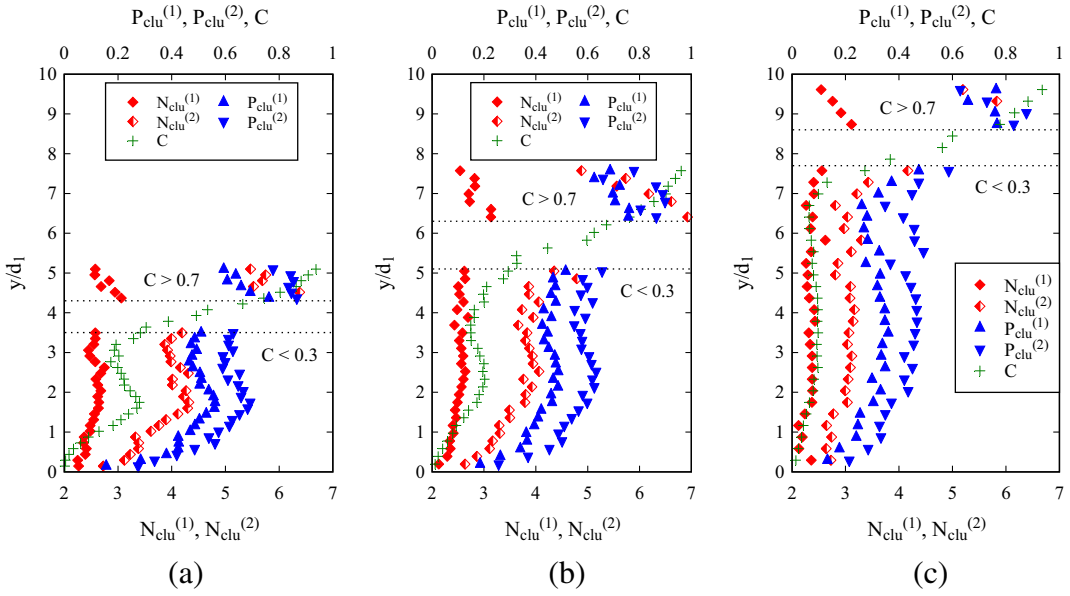

Fig. 8. Vertical distributions of longitudinal and two-dimensional cluster sizes and cluster proportions with comparison to time-averaged void fraction for Test 2 (Fr_1 = 7.5, Re = 6.8 × 10^4): (a) $(x - x_1)/d_1$ = 4.15; (b) $(x - x_1)/d_1$ = 12.5; (c) $(x - x_1)/d_1$ = 25.

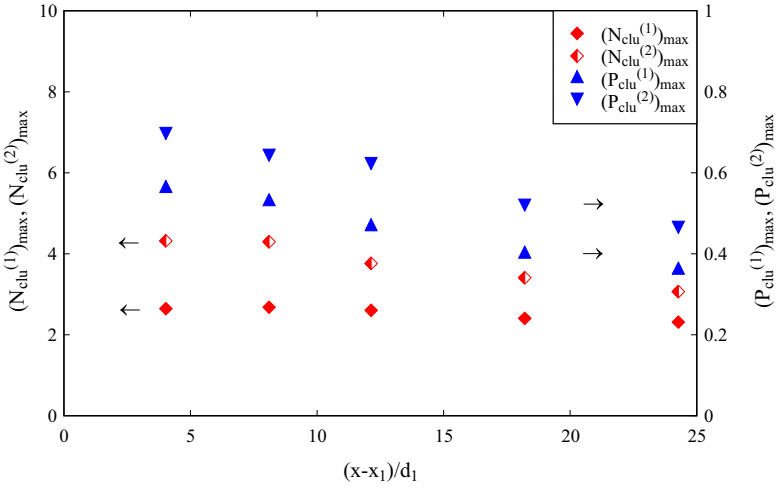

Fig. 9. Longitudinal distributions of maximum cluster sizes and maximum in turbulent shear layer for Test 2 (Fr_1 = 7.5, Re = 6.8 × 10^4).

cluster sizes $(N_{clu}{}^{(1)})_{max}$ and $(N_{clu}{}^{(2)})_{max}$ and maximum cluster proportions $(P_{clu}{}^{(1)})_{max}$ and $(P_{clu}{}^{(2)})_{max}$ are plotted in Fig. 9 as functions of the longitudinal position. Fig. 9 shows a maximum of 70% bubbles involved in two-dimensional clusters right downstream of the toe, with an average of 4.3 bubbles per cluster, and both the percentage and average number of bubbles decreased in the downstream direction. In the spray region ($C > 0.7$), the droplet cluster size and proportion decreased with decreasing water content $(1 - C)$. Note that the percentage of droplets in two-dimensional clusters reached up to 90% for $C \sim 0.7$ to 0.8, which was extremely high and was not physically observed. This is attributed to the roller surface fluctuations and will be discussed in the uncertainty section later.

When the cluster identification criterion was applied to both one-dimensional and two-dimensional, the average bubble cluster size increased by 20–60%, and the bubble cluster proportion increased by 20–40% for the given Froude number Fr_1 = 7.5. That is, a larger percentage of particles were involved in the formation of larger two-dimensional clusters. The ratios $N_{clu}{}^{(2)}/N_{clu}{}^{(1)}$ and $P_{clu}{}^{(2)}/P_{clu}{}^{(1)}$ were functions of the local void fraction C ($C < 0.3$). Further detailed information of cluster size was provided by its probability distributions. Fig. 10 shows the probability density functions of both one-dimensional and two-dimensional cluster sizes for Test 2 at the characteristic elevation of maximum bubble count rate Y_{Fmax}. For each cluster size, the data are presented at five longitudinal positions. Fig. 10 shows that the family of two-dimensional clusters consisted of a smaller proportion of two-bubble clusters (N_{clu} = 2) compared to the longitudinal clusters. Correspondingly, it contained more large-size clusters with $N_{clu} \geqslant 4$. While few longitudinal clusters consisted of more than six bubbles, such large-size clusters were observed over 10% in total two-dimensional cluster population in the first half of the roller ($(x - x_1)/d_1 \leqslant 12.5$). With increasing distance from the toe, the proportion of small-size two-dimensional clusters increased and that of large-size clusters decreased, corresponding to the dispersion of larger-scale turbulent structures and the drop in bubble

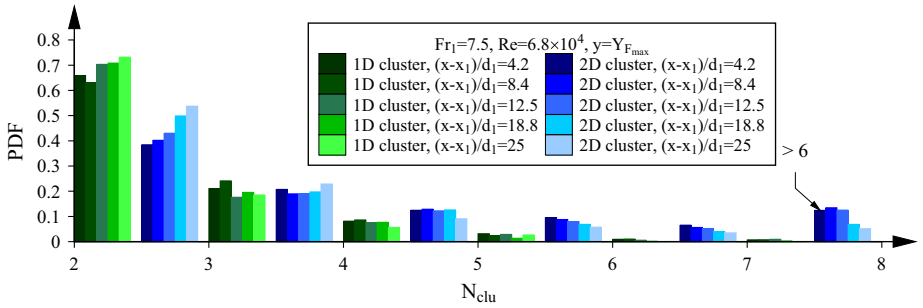

Fig. 10. Probability density functions of one-dimensional and two-dimensional cluster sizes at the elevation of maximum cluster count rate Y_{Fmax} for Test 2 (Fr_1 = 7.5, Re = 6.8 × 10^4).

concentration. Wang [26] demonstrated that, for a smaller Froude number, the longitudinal decay in the proportion of large-size clusters occurred within a shorter distance downstream of the toe.

5.3. Clustered bubble chord time

The probability distribution of bubble chord time provided information about the characteristic bubble size at a given location. Fig. 11 compares the chord time probability distributions of all bubbles and of bubbles in two-dimensional clusters, the bin size being 0.1 ms. The data were collected for Test 2 at the elevation of maximum bubble count rate Y_{Fmax}. Although both probability density functions skewed towards the class of smallest bubbles, the clustered bubbles had a smaller percentage of small bubbles compared to that in the entire bubble population. The difference was distinctive close to the toe (Fig. 11a) and became smaller at downstream (Fig. 11b). The results implied that larger bubbles had larger chance to be involved in clustering events, and the average chord length of clustered bubbles was larger than the average chord length of all bubbles given an assumption of constant velocity. Basically, a large bubble induced a large wake hence tended to affect the behaviour of adjacent bubbles.

6. Scale effects on clustering properties

A hydraulic jump is a turbulent shear flow [15], for which the Reynolds number is a critical parameter characterising the turbulent flow properties. Being a free-surface flow, the Froude number is also important. In practice, the Froude similitude is always preferred in physical modelling because of basic theoretical considerations [17,16,5]. Since it is impossible to satisfy the Froude and Reynolds similitude simultaneously using the same fluids in model and prototype, viscous scale effects may occur in down-scaled models. It is known that the turbulence-related processes such as bubble break-up and grouping undergo significant scale effects, and the air entrainment processes are affected to some extend when the Reynolds number is substantially reduced [20,8]. Herein the scale effects were investigated in terms of two-dimensional bubble clustering for four Reynolds numbers ($3.4 \times 10^4 < Re < 1.4 \times 10^5$) with an identical Froude number Fr_1 = 7.5. Please note that the transverse separation distance Δz between the phase-detection sensors was not scaled accordingly.

Fig. 12 compares the vertical distributions of two-dimensional cluster count rate (Fig. 12a), average cluster size (Fig. 12b) and cluster proportion (Fig. 12c) at the same dimensionless longitudinal position $(x - x_1)/d_1$ = 12.5 for $C < 0.3$. All properties showed typical distribution profiles, with the data magnitudes varying with the Reynolds number. The data indicated that, for a larger Reynolds number, a larger number of clusters formed and were detected per unit time (Fig. 12a), with each cluster consisting of more bubbles on average (Fig. 12b) and an increasing proportion of bubbles grouped in clusters (Fig. 12c). The bubble clustering reflected the interaction between bubbles and turbulent structures hence was strengthened by an increasing Reynolds number that characterised a higher turbulent level of the flow. In addition, the larger bubble count rate given by the increasing shear force enlarged the chance of clustering occurrence. Overall, the clustering process was relatively sensitive to the scale effects as observed by Chanson and Chachereau [8] and it should be taken into account for any scale effect assessment.

7. Discussion: selection of transverse separation Δz and uncertainties of clustering characterisation

The transverse cluster structures with bubbles travelling side by side was analysed for a specified transverse distance Δz between

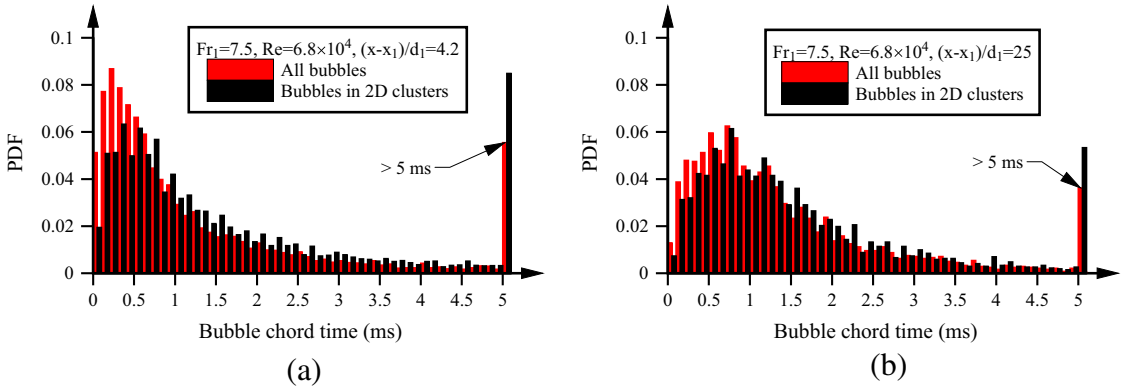

Fig. 11. Probability density functions of air chord time of all bubbles and bubbles in two-dimensional clusters at $y = Y_{Fmax}$ for Test 2 (Fr_1 = 7.5, Re = 6.8 × 10^4): (a) $(x - x_1)/d_1$ = 4.15; (b) $(x - x_1)/d_1$ = 25.

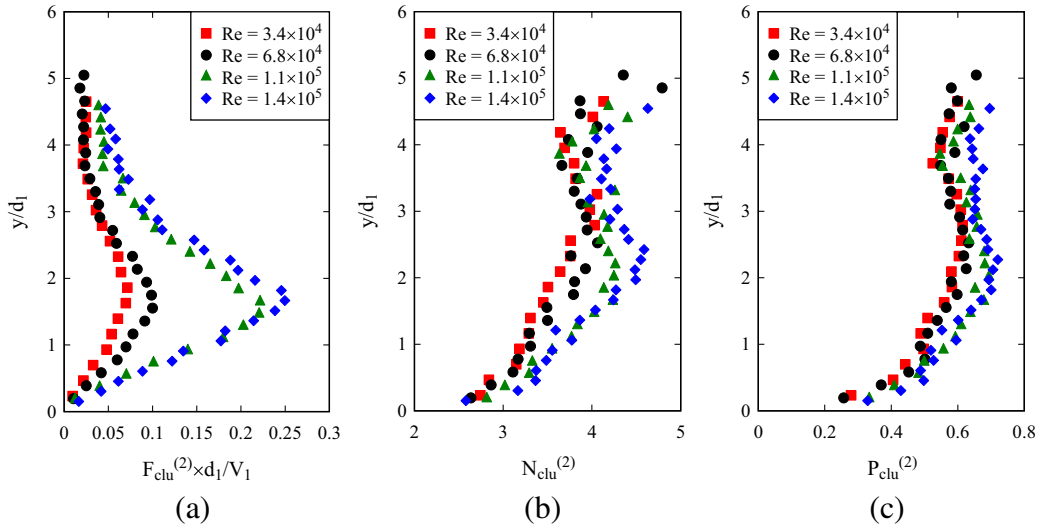

Fig. 12. Effects of Reynolds number variation on two-dimensional clustering properties in bubbly flow region; data distributions at longitudinal position $(x - x_1)/d_1 = 12.5$, $Fr_1 = 7.5$, $C < 0.3$, $\Delta z = 3.57$ mm.

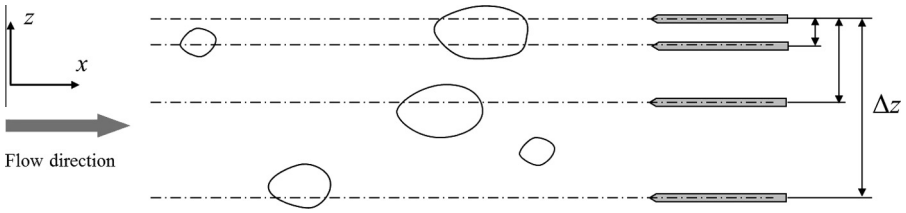

Fig. 13. Sketch of different transverse separation distances between the phase-detection sensors.

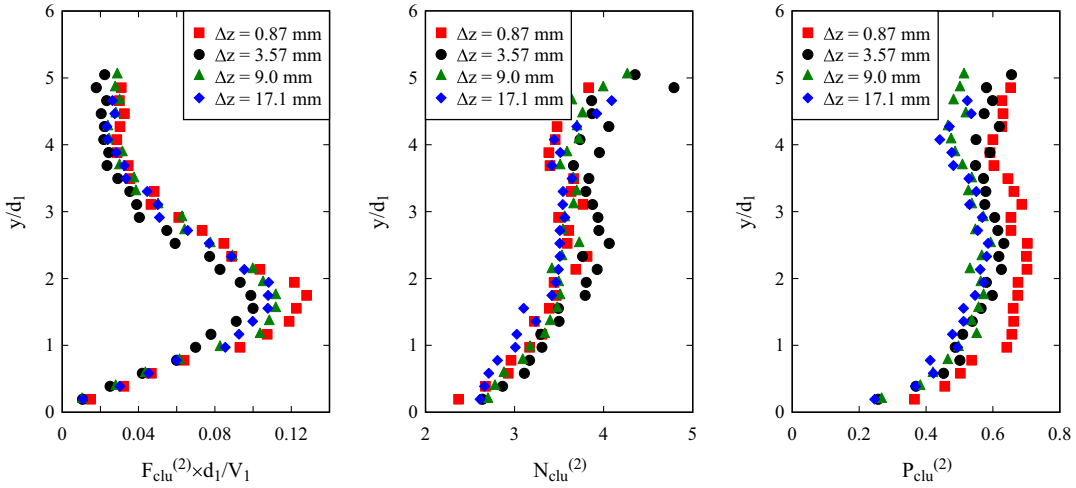

Fig. 14. Effects of transverse sensor separation distance on two-dimensional clustering properties for Test 2 ($Fr_1 = 7.5$, $Re = 6.8 \times 10^4$) at $(x - x_1)/d_1 = 12.5$, $C < 0.3$.

the phase-detection sensors (Fig. 2). The magnitudes of clustering properties were thus dependent upon the value of Δz. An appropriate selection of Δz was essential to a physically-meaningful two-dimensional clustering characterisation [25]. The separation Δz must be selected taking into account both typical particle dimensions and turbulent structure length scales. As illustrated in Fig. 13, a too small Δz increased the chance that a large bubble encountered both sensors, while the bubbles detected with a too large Δz might not directly interact with each other. Let us consider the bubbly flow in the turbulent shear region. Though the characteristic bubble chord length varied in orders of magnitudes, over 75% of the bubbles had a chord length smaller than 3 mm, among which 1/3 were found between 0.5 mm and 1 mm [26]. On the other hand, Wang et al. [27] quantified an integral turbulent length scale in the jump roller, suggesting a characteristic transverse length scale of the bubbly turbulent structures between 4 and 8 mm depending upon the longitudinal distance from the toe. As a result, a transverse separation distance Δz between 3

and 6 mm might provide an optimised transverse sensor separation. The present study applied $\Delta z = 3.57$ mm, and the effects of Δz on the clustering properties were examined for $\Delta z = 0.87$, 9.0 and 17.7 mm.

Fig. 14 presents the cluster count rate, average cluster size and cluster proportion measured with different Δz in the same vertical cross-section. Noticeable differences were seen in terms of cluster count rate and cluster proportion between the smallest Δz and the rest values. The smallest Δz gave larger cluster count rate and cluster proportion, corresponding to the frequent detection of one bubble by both sensors. Such miscount did not lead to substantial change in average cluster size. The larger transverse distances gave comparable clustering properties, implying limited dependence of clustering characterisation on the sensor separation larger than 3.57 mm. However, two sensors separated by a distance larger than 8 mm were thought to hardly capture adjacent bubbles in the shear flow region, thus the results might be physically meaningless.

Another noteworthy measurement uncertainty was related to the cluster identification next to the fluctuating roller surface. It is emphasised in Section 5.2 that the extremely large cluster proportion next to the free-surface was not meaningful. This was the result of the upwards fluctuation in water level, which instantaneously placed the phase-detection sensor in the foamy bubbly flow. In this case, the droplet clustering criterion (Eqs. (3) and (4)) was applied to the bubbly flow with air bubbles being the actual clustering particles, yielding to a large number of "fake" clusters. The projections of foamy air–water entities (see Fig. 1b) also contributed to such "fake" clusters even when the void fraction reached above 0.8.

8. Conclusion

The clustering of air bubbles and water droplets in hydraulic jumps was studied based upon a two-dimensional near-wake clustering criterion. Bubble–bubble interactions were examined between adjacent bubbles travelling one after another or side by side. The clustering properties were characterised in terms of the cluster count rate, cluster size, cluster proportion and clustered bubble chord time. Full data profiles were obtained through vertical cross-sections on the roller centreline. Comparisons were made between the clustering properties and basic air–water flow properties, as well as between the results derived from the two-dimensional clustering criterion and from the traditional one-dimensional criterion.

The cluster count rate was quasi-proportional to the bubble count rate. A local maximum was exhibited at the same vertical position of maximum bubble count rate in the turbulent shear layer. The vertical distributions of average cluster size and cluster proportion showed similar shapes to the time-averaged void fraction profile in the bubbly flow, both reaching local maxima close to the elevation of maximum void fraction. In the highly-aerated flow region downstream of the toe, over 50% of bubbles were transported in two-dimensional clusters. Though the largest percentage of clusters was formed by two bubbles, over 10% of clusters were large two-dimensional clusters that consisted of six bubbles or more. All clustering properties decreased in the longitudinal direction as the turbulence dissipated and flow de-aerated. The average size of clustered bubbles was larger than that of the entire bubble population. The clustering process was linked closely to the turbulence development hence all clustering properties were sensitive to the scale effects.

Compared to the traditional longitudinal cluster definition, the simultaneous consideration of longitudinal and transverse cluster structures enlarged the average cluster size by 20–60% and the percentage of clustered bubbles by 20–40%, whereas the number of clusters over the same period of time was reduced. The most distinctive difference was observed close to the jump toe where the formation of three-dimensional turbulent structures was intense. Overall, the present study indicated an intensive occurrence of two-dimensional particle clustering in the hydraulic jump roller. The clustering process was a reflection of the interaction between bubble convection and turbulence dissipation. The clustering properties thus provided some valuable measure of the bubble–turbulence interplay in such complex air–water flows. Complementary information about the structure of each cluster and the range of bubbles sizes affected by clustering may be further obtained in future studies by applying inter-particle arrival time analysis (IATA) to two-dimensional clusters.

Acknowledgements

The authors acknowledge the input of Dr Frédéric Murzyn (ESTACA Laval, France). They thank Jason Van Der Gevel and Stewart Matthews, School of Civil Engineering, The University of Queensland for their technical assistance. The authors acknowledge the financial support of the Australian Research Council (Grant DP120100481).

References

[1] E. Calzavarini, T.H. van der Berg, F. Toschi, D. Lohse, Quantifying microbubble clustering in turbulent flow from single-point measurements, Phys. Fluids 20 (4) (2008) 6 pages, http://dx.doi.org/10.1063/1.2911036. Paper 040702.
[2] Y. Chachereau, H. Chanson, Bubbly flow measurements in hydraulic jumps with small inflow Froude numbers, Int. J. Multiph. Flow 37 (6) (2011) 555–564, http://dx.doi.org/10.1016/j.ijmultiphaseflow.2011.03.012.
[3] H. Chanson, Air Bubble Entrainment in Free-Surface Turbulent Shear Flows, Academic Press, London, UK, 1997. 401 pages.
[4] H. Chanson, Bubbly flow structure in hydraulic jump, Eur. J. Mech. B. Fluids 26 (3) (2007) 367–384, http://dx.doi.org/10.1016/j.euromechflu.2006.08.001.
[5] H. Chanson, Momentum considerations in hydraulic jumps and bores, J. Irrig. Drain. Eng. 138 (4) (2012) 382–385, http://dx.doi.org/10.1061/(ASCE)IR.1943-4774.0000409.
[6] H. Chanson, S. Aoki, A. Hoque, Bubble entrainment and dispersion in plunging jet flows: freshwater versus seawater, J. Coastal Res. 22 (3) (2006) 664–677, http://dx.doi.org/10.2112/03-0112.1.
[7] H. Chanson, T. Brattberg, Experimental study of the air–water shear flow in a hydraulic jump, Int. J. Multiph. Flow 26 (4) (2000) 583–607.
[8] H. Chanson, Y. Chachereau, Scale effects affecting two-phase flow properties in hydraulic jump with small inflow Froude number, Exp. Thermal Fluid Sci. 45 (2013) 234–242, http://dx.doi.org/10.1016/j.expthermflusci.2012.11.014.
[9] H. Chanson, L. Toombes, Air–water flows down stepped chutes: turbulence and flow structure observations, Int. J. Multiph. Flow 28 (11) (2002) 1737–1761.
[10] S. Felder, Air–water flow properties on stepped spillways for embankment dams: aeration, energy dissipation and turbulence on uniform, non-uniform and pooled stepped chutes, PhD thesis, School of Civil Engineering, The University of Queensland, Brisbane, Australia, 2013, 454 pages.
[11] C. Gualtieri, H. Chanson, Clustering process analysis in a large-size dropshaft and in a hydraulic jump, in: G. Di Silvio, S. Lanzoni, (Ed.), Proceedings of the 32nd IAHR Biennial Congress, Venice, Italy, 2007, 11 pages.
[12] C. Gualtieri, H. Chanson, Effect of Froude number on bubble clustering in a hydraulic jump, J. Hydraul. Res. 48 (4) (2010) 504–508, http://dx.doi.org/10.1080/00221686.2010.491688.
[13] J. Heinlein, U. Fritsching, Droplet clustering in sprays, Exp. Fluids 40 (3) (2006) 464–472.
[14] F.M. Henderson, Open Channel Flow, MacMillan Company, New York, USA, 1966.
[15] J.W. Hoyt, R.H.J. Sellin, Hydraulic jump as 'mixing layer', J. Hydraul. Eng. 115 (12) (1989) 1607–1614.
[16] J.A. Liggett, Fluid Mechanics, McGraw-Hill, New York, USA, 1994.
[17] J. Lighthill, Waves in Fluids, Cambridge University Press, Cambridge, UK, 1978. 504 pages.
[18] D. Long, N. Rajaratnam, P.M. Steffler, P.R. Smy, Structure of flow in hydraulic jumps, J. Hydraul. Res. 29 (2) (1991) 207–218.
[19] F. Murzyn, Assessment of different experimental techniques to investigate the hydraulic jump: do they lead to the same results? in: R. Janssen, H. Chanson, (Ed.), Proceedings of 3rd International Junior Researcher and Engineer Workshop on Hydraulic Structures, May 2–3, 2010, Edinburgh, Scotland, Hydraulic Model Report CH80/10, School of Civil Engineering, the University of Queensland, Brisbane, Australia, 2010, pp. 3–36.

[20] F. Murzyn, H. Chanson, Experimental assessment of scale effects affecting two-phase flow properties in hydraulic jumps, Exp. Fluids 45 (3) (2008) 513–521, http://dx.doi.org/10.1007/s00348-008-0494-4.
[21] F. Murzyn, D. Mouaze, J.R. Chaplin, Optical fibre probe measurements of bubbly flow in hydraulic jumps, Int. J. Multiph. Flow 31 (1) (2005) 141–154.
[22] N. Rajaratnam, An experimental study of air entrainment characteristics of the hydraulic jump, J. Inst. Eng. India 42 (7) (1962) 247–273.
[23] N. Rajaratnam, Hydraulic jumps, in: V.T. Chow (Ed.), Advances in Hydroscience, vol. 4, Academic Press, N.Y., 1967, pp. 197–280.
[24] F.J. Resch, H.J. Leutheusser, Le ressaut hydraulique: mesure de turbulence dans la région diphasique. (The hydraulic jump: turbulence measurements in the two-phase flow region.), J. La Houille Blanche 4 (1972) 279–293 (in French).
[25] S. Sun, H. Chanson, Characteristics of clustered particles in skimming flows on a stepped spillway, Environ. Fluid Mech. 13 (1) (2013) 73–87, http://dx.doi.org/10.1007/s10652-012-9255-2.
[26] Wang, Turbulence and Air Entrainment in Hydraulic Jumps, PhD thesis, School of Civil Engineering, The University of Queensland, Brisbane, Australia, 2014, 303 pages.
[27] H. Wang, S. Felder, H. Chanson, An experimental study of turbulent two-phase flow in hydraulic jumps and application of a triple decomposition technique, Exp. Fluid 55 (7) (2014), http://dx.doi.org/10.1007/s00348-014-1775-8. Paper 1775, 18 pages & 2 video movies.